Acoustic Receptivity Measurements Using Modal Decomposition of a Modified Orr–Sommerfeld Equation

Jason A. Monschke*, Matthew S. Kuester*, and Edward B. White†

Department of Aerospace Engineering
Texas A&M University
College Station, TX 77843–3141

Boundary-layer receptivity to acoustic disturbances plays a key role in transition from laminar to turbulent flow. Acoustic disturbances interact with strong streamwise gradients in the boundary layer to create Tollmien–Schlichting (T–S) waves. Measurement of T–S waves created by downstream-traveling sound is complicated by the presence of Stokes waves in the boundary layer. Upstream-traveling acoustic reflections also generate T–S waves at the leading edge which are indistinguishable from T–S waves originating from downstream-traveling waves. In this experiment, active noise control is used to cancel reflections and enables the measurement of boundary-layer receptivity to downstream-traveling sound. T–S wave amplitudes are then extracted from hotwire data using biorthogonal decomposition of modified Orr–Sommerfeld (O–S) equations that include Stokes waves as a solution. The new method is implemented to measure the acoustic receptivity of a 20:1 modified-super-ellipse (MSE) leading edge on a flat plate. The data yield an acoustic receptivity curve with a larger amplitude than the results of previous computational studies, but the maximum occurs at the same nondimensional frequency. The new measurement technique provides for efficient decomposition of measurements and sets the stage for renewed experimental effort in this area.

Nomenclature

$\bar{x}_{vle}$	Virtual leading edge location with respect to physical leading edge (m)
$\bar{x}$	Streamwise distance from virtual leading edge (m)
x	Nondimensional streamwise distance from virtual leading edge
f	Forcing frequency (Hz)
t	Time (s)
ν	Kinematic viscosity (m^2/s)
U_∞	Freestream velocity (m/s)
M_∞	Freestream Mach number
R_b	Reynolds number based on half plate width
F	$2\pi f\nu/U_\infty^2$, Nondimensional frequency
R	$\sqrt{U_\infty \bar{x}/\nu}$, Reynolds number based on the boundary-layer length scale
N	Amplification factor
U	Nondimensional basic state streamwise velocity
P	Nondimensional basic state pressure
δ^*	Boundary-layer displacement thickness (m)
θ	Boundary-layer momentum thickness (m)

*Graduate Research Assistant, AIAA Student Member
†Associate Professor, AIAA Assc. Fellow

H	δ^*/θ, Boundary-layer shape factor
α	Nondimensional streamwise wavenumber
δ_r	$\sqrt{\nu\bar{x}/U_\infty}$, Boundary-layer length scale (m)
y	Dimensional wall-normal coordinate (m)
η	y/δ_r, Nondimensional wall-normal coordinate
$\tilde{y}$	Independent variable in the Chebyshev domain
u'	Fluctuating streamwise velocity component in the time domain
$\hat{u}$	Fluctuating streamwise velocity component in Fourier space
$\hat{v}$	Fluctuating wall-normal velocity component in Fourier space
$\hat{p}$	Fluctuating pressure in Fourier space
$\mathcal{A}$	Left modified Orr–Sommerfeld matrix operator
$\mathcal{B}$	Right modified Orr–Sommerfeld matrix operator
$\vec{\phi}$	Vector of perturbation quantities
$\vec{\psi}$	Vector of adjoint quantities
D	Partial derivative operator with respect to wall-normal coordinate
Q_α	Biorthogonality normalization constant for streamwise wavenumber, α
Q_{TS}	Tollmien–Schlichting wave biorthogonality normalization constant
Q_{St}	Stokes wave biorthogonality normalization constant
C_{TS}	Complex Tollmien–Schlichting wave amplitude
C_{St}	Complex Stokes wave amplitude
K_I	Acoustic receptivity coefficient defined at branch I

I. Introduction

UNDERSTANDING and controlling boundary-layer transition from laminar to turbulent flow is critical for numerous aerodynamics applications. For example, the reduction in skin friction drag for laminar flow compared to turbulent flow could provide a substantial savings in fuel and weight for a commercial airliner. In spite of its importance, transition is still not fully understood. Because of the open-flow nature of these types of systems, boundary-layer transition is initiated when irrotational (sound) and rotational (turbulence) disturbances interact with a surface and create boundary-layer fluctuations. This process, called receptivity, is important because it sets the initial amplitudes of disturbances which grow and eventually lead to turbulent flow. This path from laminar to turbulent flow is concisely summarized in Morkovin's[1] transition road map, Figure 1. Receptivity has been a focus of the boundary-layer stability community for over 40 years, but the process of how disturbances become entrained in the boundary layer is still not well understood. Understanding the receptivity process will further our ability to avoid or control boundary-layer transition.

The receptivity of planar, two-dimensional sound has been addressed by theory,[2] experiments,[3–6] and direct numerical simulation (DNS).[7–10] Theoretical studies utilizing triple deck theory and the unsteady-boundary-layer equations showed that the interaction of freestream disturbances with large streamwise gradients at the leading edge creates unstable waves that match the behavior of T–S waves as they travel downstream.[2] T–S waves are a solution to the Orr–Sommerfeld (O–S) equation, shown in Eq. (1), which governs small disturbances in a parallel basic state.

$$\mathcal{A}\frac{\partial\vec{\phi}}{\partial\eta} = \mathcal{B}\vec{\phi} \tag{1}$$

$$\vec{\phi} = \left[\hat{u}, \quad \frac{\partial\hat{u}}{\partial\eta}, \quad \hat{v}, \quad \hat{p}, \quad \frac{\partial\hat{u}}{\partial x}, \quad \frac{\partial\hat{v}}{\partial x}\right]^T$$

$\mathcal{A}$ and $\mathcal{B}$ are 6×6 matrix operators shown in the Appendix, variables with hats denote variables in Fourier space, and a superscript T indicates the transpose operator. The O–S equation is an eigenvalue problem for the streamwise wavenumber (α). The O–S operators have been written so that the streamwise wavenumber appears linearly. For a given frequency (F), Reynolds number (R), and basic state ($U(\eta)$), the O–S equation is solved using a Chebyshev collocation method.[11] The physical domain, $\eta = [0, \eta_{max}]$, is mapped into the Chebyshev domain, $\tilde{y} = [-1, 1]$, using a mapping that concentrates the collocation points in a region near the wall. If the imaginary portion of α is less than zero, the mode is spatially unstable and grows as it travels

downstream. In this paper, only two-dimensional disturbances with $w = 0$ and $\partial/\partial z = 0$ are considered.

T–S waves are unstable over a range of Reynolds numbers. At constant nondimensional frequency, F, the Reynolds number where instability first occurs is the branch I Reynolds number. The Reynolds number where the T–S wave becomes stable again is the branch II Reynolds number. In-between branch I and branch II, T–S waves grow as they travel downstream. During this growth, nonlinear interactions may occur, which eventually cause the boundary layer to transition to turbulence. Understanding how acoustic fluctuations become entrained in the boundary layer and create T–S waves will be a fundamental building block in understanding the transition process.

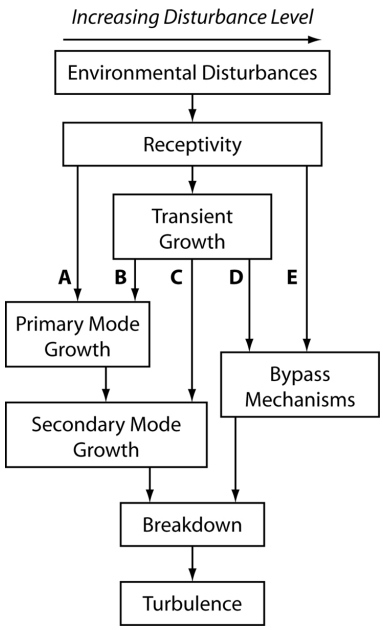

Figure 1. The path from laminar to turbulent flow summarized in the transition roadmap by Morkovin.[1]

Experiments at Arizona State University (ASU),[3–6] coupled with matching DNS studies,[7–10] have investigated acoustic receptivity by introducing planar freestream sound into the test environment and measuring the amplitude of T–S waves near the branch II Reynolds numbers. Early experiments used continuous acoustic forcing, while later experiments used pulsed-sound forcing. Both techniques have drawbacks. Continuous forcing creates measurement issues and contaminates the experiment through complex duct acoustics and wake resonance.[4] Pulsed forcing requires a large number of ensemble averages and has poor frequency resolution.[6]

This paper will describe a T–S wave measurement technique involving modal decomposition of a modified O–S equation. This technique has several advantages over previous methods, and, combined with active noise control, enables the use of continuous forcing. Finally, the modal decomposition technique is utilized to experimentally measure leading-edge acoustic receptivity coefficients.

The acoustic receptivity of certain leading edge geometries has been studied extensively, but these measurements need to be extended to more practical flow fields. For example, receptivity theory[12] and computations[13] have analyzed the receptivity of parabolic leading edges at non-zero angles of attack, but these observations have not been validated by experiments. It is anticipated that the approach developed here will be a reliable, efficient method for measuring T–S waves and making receptivity measurements and will help to extend our knowledge of the receptivity process to more complicated geometries.

II. Acoustic Receptivity Techniques

The presence of Stokes waves (acoustic boundary layers) presents a challenge while measuring boundary-layer receptivity to acoustic disturbances. In the case of continuous acoustic forcing, a hotwire placed in the boundary layer will detect a combination of T–S waves, Stokes waves, and sting vibration effects. Because all three phenomena occur at the same frequency, using a narrow band-pass filter will not separate the T–S wave from either source of contamination. Several separation techniques have been developed to measure T–S wave amplitudes, but each method has drawbacks. A new method for measuring T–S wave amplitudes is proposed that utilizes the biorthogonal properties of a modified O–S equation.

A. Complex Plane Spiral Analysis

Saric et al.[3] utilized a complex plane analysis technique to measure receptivity coefficients. Because the acoustic wavelength is orders of magnitude larger than the T–S wavelength, the Stokes wave has nearly a constant phase over one T–S wavelength. Hotwire measurements are taken at several streamwise locations across one T–S wavelength, and the real and imaginary components of the velocity signal are plotted in the complex plane. The radius of the spiral in the complex plane is the amplitude of the T–S wave, while the contributions due to sting vibration and the Stokes wave are constants that offset the spiral from the origin.

There are several drawbacks to this method. A large number of measurements are needed to obtain just one T–S wave measurement. For example, to complete a single amplitude measurement at a single height in the boundary layer requires measurements at multiple streamwise locations. Finally, continuous acoustic forcing creates a complex acoustic field in the test section. A portion of the forcing acoustic wave is reflected

by the change of cross-section area downstream of the test section. Goldstein's analysis[2] suggests that the receptivity to upstream-traveling waves is greater than downstream-traveling waves, so the presence of the diffuser reflection can affect the receptivity measurement. Saric & White[4] also noted a global circulation effect in the test section during continuous forcing. This effect, which may be caused by wake resonance described by Takagi and Konishi,[14] can artificially enhance certain bands of T–S waves. Overall, the complex plane technique is tedious and has challenges associated with continuous acoustic forcing.

B. Pulsed-Sound Technique

White et al.[6] and Saric & White[4] use a pulsed-sound technique to separate Stokes and T–S waves. The pulsed-sound technique utilizes the differences in group velocity of the two waves; the Stokes wave travels at the speed of sound, while the T–S wave travels downstream at a fraction of the freestream velocity. Sound is emitted from speakers upstream of the model in a short burst (two to four cycles), and this sound interacts with the leading edge to create a packet of T–S waves. The Stokes waves rapidly pass the measurement location, and after a short delay, the T–S waves pass the measurement location. Data acquisition is timed such that the boundary-layer hotwire acquires data once the Stokes waves have passed. Large numbers of ensemble averages are used to account for low-frequency oscillations in the flow, and the receptivity coefficient is calculated in the frequency domain through the separate averaging of real and imaginary parts.

Although this technique removes the effects of Stokes waves, the number of ensemble averages required is cumbersome. Obtaining one boundary layer profile can require many hours of measurement.[6] Another drawback of this technique is the lack of frequency resolution. The forcing sound wave is a short burst of sine wave cycles, the Fourier transform of which contains a broad range of frequencies. The receptivity coefficient is calculated in the frequency domain, but the length of the sampling window is limited by the timing of the Stokes and T–S waves. The number of samples in the sampling window limits the frequency resolution of this technique. Although the pulsed-sound method avoids the wake resonance problem, diffuser reflections are present and may still contaminate the measurements. Furthermore, there are significant differences between the pulsed-sound results of White et al.[6] and Saric & White.[4] Specifically, the receptivity coefficient appears to be a strong function of freestream velocity. Due to the small number of experimental measurements, it is not clear if this trend is physical or an artifact of the pulse-sound method.

C. Modal Decomposition

Denissen & White[15] recently investigated roughness induced transient growth using biorthogonal decomposition to compute the amplitude and phases of continuous modes of the O–S equation. In this method, experimental or DNS data is used to find the coefficients of the modes of the O–S equation that, when combined, create the disturbance profile. In a similar fashion, Stokes waves can be separated from T–S waves through modal decomposition. Stokes waves, like T–S waves, are small perturbations upon the parallel basic state. As such, Stokes waves should be governed by a modified O–S equation. If the modified O–S equation can be cast in such a way that both T–S waves and Stokes waves are solutions, then the biorthogonal nature of the direct and adjoint solutions to the modified system of equations can be utilized to separate the different modes.

The O–S equation governs small fluctuations on an incompressible flow with a parallel basic state. By nature, acoustic waves are not incompressible. In order for Stokes waves to be captured by the O–S equation, the continuity equation must be modified to account for dilation effects. For the derivation of the modified O–S equation, the basic state is assumed to be parallel and incompressible, but density perturbations are allowed. The Mach number appears in the equations to introduce the acoustic length scale.

The standard boundary conditions for the O–S equation are zero velocity fluctuations ($\hat{u} = \hat{v} = 0$) at the wall and the freestream for a total of four boundary conditions. Two boundary conditions are modified to admit Stokes wave solutions of the modified equations:

- instead of $\hat{u} = 0$, $\partial\hat{u}/\partial\eta = 0$ in the freestream
- instead of $\hat{v} = 0$ in the freestream, require the non-zero $\hat{u}$ to be offset by dilation effects

T–S waves are still captured by the modified boundary conditions because $\hat{u}$ and $\hat{v}$ asymptotically approach zero in the freestream. For a given Reynolds number and nondimensional frequency, T–S waves computed using the two O–S equations (standard equations and boundary conditions, modified equations

and relaxed boundary conditions) produce the same eigenvalue (α) and the same mode shape. Computations with the relaxed boundary conditions also produce upstream- and downstream-traveling Stokes waves. Because of the added dilation effects in the continuity equation, the streamwise wavenumber of the Stokes wave equals the freestream acoustic wavelength at the forcing frequency.

Stokes waves and T–S waves have been cast as solutions to the same eigenvalue problem. Therefore, the amplitudes of the T–S waves and the Stokes waves can be extracted through the biorthogonality relationships shown in Eqs. (2) and (3). The general approach follows that of Tumin et al.[16] who developed it for a two-dimensional wall jet. A derivation of these relationships is given in the Appendix.

$$C_{TS} = \frac{1}{Q_{TS}} \left\langle \vec{\phi}, \vec{\psi}_{TS} \right\rangle \Big|_0^\infty \tag{2}$$

$$C_{St} = \frac{1}{Q_{St}} \left\langle \vec{\phi}, \vec{\psi}_{St} \right\rangle \Big|_0^\infty \tag{3}$$

In Eqs. (2) and (3), $\vec{\phi}$ is the full set of velocity and pressure data, $\vec{\psi}_{TS}$ is the T–S wave solution to the adjoint modified O–S equation, and $\vec{\psi}_{St}$ is the Stokes wave solution to the adjoint modified O–S equation. The adjoint modified O–S equation is shown, along with boundary conditions, in Eq. (4). Q_{TS} and Q_{St} are normalizing constants obtained by applying the biorthogonality relationship to the Stokes and T–S wave solutions of Eqs. (1) and (4).

$$\begin{gathered} \mathcal{A}\frac{\partial \vec{\psi}}{\partial \eta} = -\mathcal{B}^T \vec{\psi} \\ \psi_2|_0 = 0, \quad \psi_4|_0 = 0, \quad \psi_3|_\infty = 0 \\ -M_\infty^2 \left[\alpha U - RF\right] \psi_1|_\infty + \alpha \left(1 - iM_\infty^2 F\right) \psi_4|_\infty + \alpha M_\infty^2 U \psi_6|_\infty = 0 \end{gathered} \tag{4}$$

The only component of $\vec{\phi}$ that can be measured experimentally is the streamwise component $\hat{u}$. Other needed components cannot be measured accurately in an experiment. Tumin et al.[16] used a superposition of two mode shapes to assume a form for the unknown quantities in the state vector of a wall jet. This method, however, does not work well for finding the amplitude of T–S waves in the presence of Stokes waves. A somewhat different approach is to decompose the Stokes and T–S waves separately.

Because the decomposition algorithm considers Stokes and T–S waves separately, the unknown quantities are assumed to be a Stokes when finding C_{St}, or a T–S wave when finding C_{TS}. To begin the decomposition, the Stokes wave amplitude is found using the experimental data, $\hat{u}_{exp}$, a Stokes wave modal assumption, and Eq. (3). The decomposed Stokes wave is then subtracted from $\hat{u}_{exp}$. After removing the Stokes wave from the experimental signal, $\hat{u}_{exp}$ now almost entirely consists of the T–S wave and noise. The T–S wave amplitude is then calculated by applying the biorthogonality condition to this updated $\hat{u}_{exp}$ and a T–S wave modal assumption. This method can also be extended for data sets that do not extend to the wall and have finite extent into the freestream. Details of this algorithm are contained within the Appendix.

The modal decomposition technique has several advantages over the previously mentioned experimental techniques. By sampling one boundary-layer profile (with consistent phase relative to the input), the T–S wave amplitude can be measured quickly without moving to another streamwise location. This is a significant increase in efficiency over previous methods. Because single frequencies are used, this technique does not have the frequency resolution problems associated with the pulsed-sound technique.

III. Experimental Facility & Setup

The receptivity measurements were performed in the Klebanoff–Saric Wind Tunnel (KSWT) at Texas A&M University. The KSWT is a low disturbance, low speed wind tunnel specifically designed for boundary-layer stability and transition work. A complete description of the tunnel, including flow quality, is given by Hunt et al.[17] During construction, broadband acoustic panels and acoustic foam were added inside the tunnel to lower background flow noise from the fan and motor. These acoustic treatments were chosen specifically to reduce noise in the T–S passband. Sound is introduced to the test environment from five McCauley subwoofers mounted upstream of the test section. The subwoofers emit near-planar sound that interacts with the model to create T–S waves. To prevent nonlinear effects, the sound amplitude is limited to 100 dB within the test section.

A. Flat-Plate Model

The model used is an aluminum-nickel alloy flat plate with a 20:1 modified-super-ellipse (MSE) leading edge.[8] The plate is 9.53 mm thick, 4000 mm long, and 1370 mm wide. The leading edge is located approximately 690 mm from the contraction. The MSE leading edge eliminates the discontinuity in surface curvature at the leading-edge/flat-plate juncture, which is a possible receptivity location. To further ensure that the interface is smooth, the leading edge has been machined directly on the flat plate.

The flat plate is mounted vertically in the test section, off-center (56:44). Five adjustable mounting brackets allow for fine alignment to ensure $\partial P/\partial x = 0$. Following the recommendation by Saric,[18] the flat-plate is aligned so that $H = \delta^*/\theta = 2.59 \pm 0.005$. Plate alignment is crucial to ensure that the N-factor growth rates match linear stability theory for Blasius flow. A 500 mm trailing-edge flap is used to adjust the location of the stagnation line. Differential pressure sensors on either side of the leading edge are used to ensure symmetric flow. A Velcro strip located on the non-test side of the plate fixes the transition location and ensures constant blockage.

Due to non-zero pressure gradients near the leading-edge, the streamwise coordinate is referenced to the virtual leading edge, $\bar{x}_{vle}$. The virtual leading edge is found through a least squares fit to the growth of the momentum thickness to be 55 ± 9 mm downstream of the physical leading edge.

B. Active Noise Control

One of the major challenges involved with continuous acoustic forcing is the complex duct acoustics involved with closed loop wind tunnels. The continuous forcing creates a standing wave pattern in the test section due to a reflection from the diffuser downstream of the test section. This standing wave can create an interference pattern that can distort receptivity measurements. The reflection from the diffuser can also cause wake resonance which can cause a frequency selection effect. Goldstein[2] showed that the leading edge is much more receptive to upstream-traveling waves than downstream. Sound waves traveling in both directions generate T–S waves at the leading edge, and thus the T–S waves created by downstream-traveling sound are inseparable from the T–S waves created by upstream-traveling sound.

For this work, the diffuser reflection is eliminated using an active noise control strategy developed by Kuester & White.[19] Two secondary subwoofers downstream of the test section emit sound waves that actively cancel the reflection from the diffuser using closed loop control. A finite impulse response (FIR) filter is used to filter the signal sent to the primary subwoofers; the filtered signal is sent to the secondary subwoofers in order to cancel upstream-traveling waves. Four microphones at different streamwise locations in the test section separate upstream-traveling and downstream-traveling sound; a gradient descent algorithm then updates the FIR filter to an optimum value such that the upstream-traveling sound is minimized. Kuester & White[19] provide details of the active noise control setup.

Before performing the receptivity experiments, the active noise control system was tested at multiple frequencies at the tunnel test conditions. Figure 2 shows the upstream- and downstream-traveling sound waves that were decomposed by two sets of microphones at the same streamwise location. For this measurement, the speaker wall was excited with sine waves at a constant forcing amplitude. Squares indicate upstream-traveling waves, while circles indicate downstream-traveling waves. The solid lines indicate the baseline case (active noise control off), and dashed lines indicate the controller-on case. The downstream-traveling waves are not strongly affected by the controller, while the upstream-traveling waves were reduced on average by 20.4 dB. Using active noise control allows continuous acoustic forcing, and thus modal decomposition of fluctuating velocity profiles in the measurement of leading-edge acoustic receptivity.

C. Receptivity Measurement Technique

For a given frequency, a wall normal hotwire scan is performed at the branch II location on the flat plate. The T–S wave is measured at the branch II location in order to let the disturbance grow to maximum amplitude so that the signal-to-noise ratio can be maximized. All measurements are taken with a constant Reynolds number based on the half-width of the plate, $R_b = 2430$, to match previous computational studies.[10] To avoid the issue of frequency bins associated with a Fourier transform, a least-squares fit of a normal mode is applied to the time-varying hotwire data. The resulting $\hat{u}$ is then phase-locked with the function generator signal used to drive the upstream speaker wall.

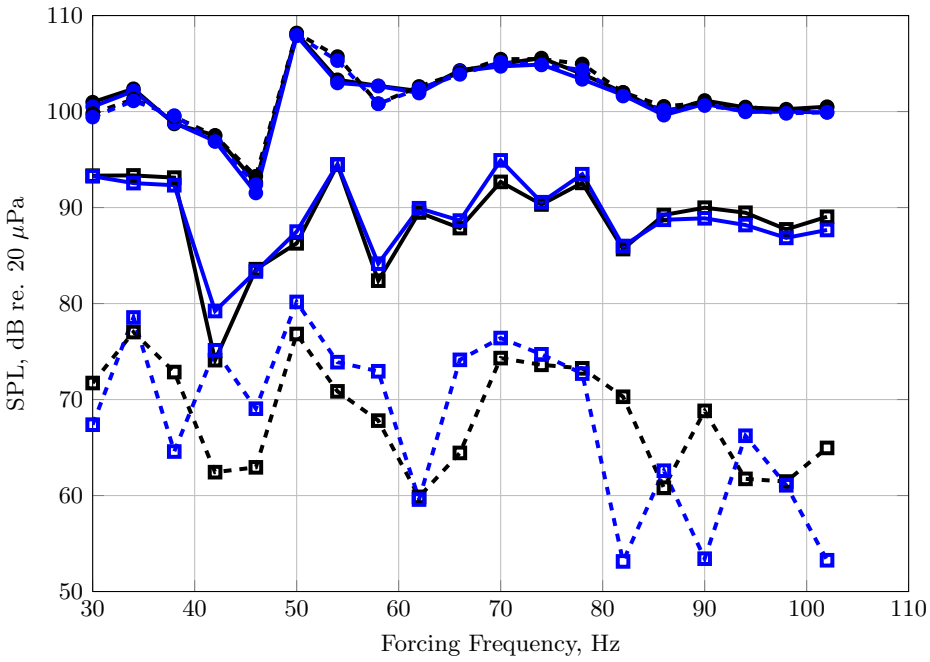

Figure 2. The active noise control system reduces the amplitude of upstream-traveling waves on average by 20.4 dB without affecting the downstream-traveling waves. Squares indicate upstream-traveling waves and circles indicate downstream-traveling waves. Also, solid lines indicate the baseline case and dashed lines indicate the controller-on case.

After determining the amplitude of the T–S wave through modal decomposition, the receptivity coefficient is defined by scaling the amplitude to its branch I value and dividing by the amplitude of the freestream sound wave at the leading edge.

$$K_I = \frac{(|\hat{u}|_{TS})_{BranchI}}{(|\hat{u}|_{St})_{LE}} = \frac{(|\hat{u}|_{TS})_{BranchII}}{e^N\,(|\hat{u}|_{St})_{LE}} \tag{5}$$

IV. Results

In the past, wake resonance has restricted the use of continuous forcing in acoustic receptivity experiments.[3] Presently, active noise control is used to eliminate upstream-traveling sound and the wake resonance effect. To measure the effect of wake resonance, hotwires are placed on both sides of the flat plate at the same streamwise location. The fluctuating velocity component, $\hat{u}$, at the frequency of interest is computed for each wire. Comparing the amplitudes and phases of each fluctuating velocity reveals a frequency selection effect (large, sharp peaks in relative phase and amplitude) similar to what is seen in receptivity coefficients by Saric et al.[3] Thus, global circulation may be an additional receptivity source. However, no evidence is seen in the receptivity results presented below. Insight into the illusive phenomenon known as wake resonance has been gained through this research, but, more work is needed to fully understand the relationship between continuous forcing, wake resonance, and the effect on acoustic receptivity experiments. With the caveats above, the following acoustic receptivity results are presented.

Figure 3 shows the biorthogonal decomposition results for the nondimensional frequency $F = 93.2\times10^{-6}$, which is also the frequency of maximum acoustic receptivity at $R_b = 2430$. This plot is a representative sample of each decomposition. The plot makes clear that the experimental decomposition method accurately extracts the correct amplitude and phase of both Stokes and T–S waves.

Because the receptivity coefficient is measured at the branch II location and scaled to the branch I location using linear stability theory, it is imperative that there is no streamwise pressure gradient and that the streamwise growth of T–S waves matches linear stability theory. To verify this, Kapton tape was placed at the branch I point on the plate and the speaker wall/tunnel were set to achieve a nondimensional frequency of $F = (56.8 \pm 0.2) \times 10^{-6}$ with the goal of generating large amplitude T–S waves. Because the T–S waves

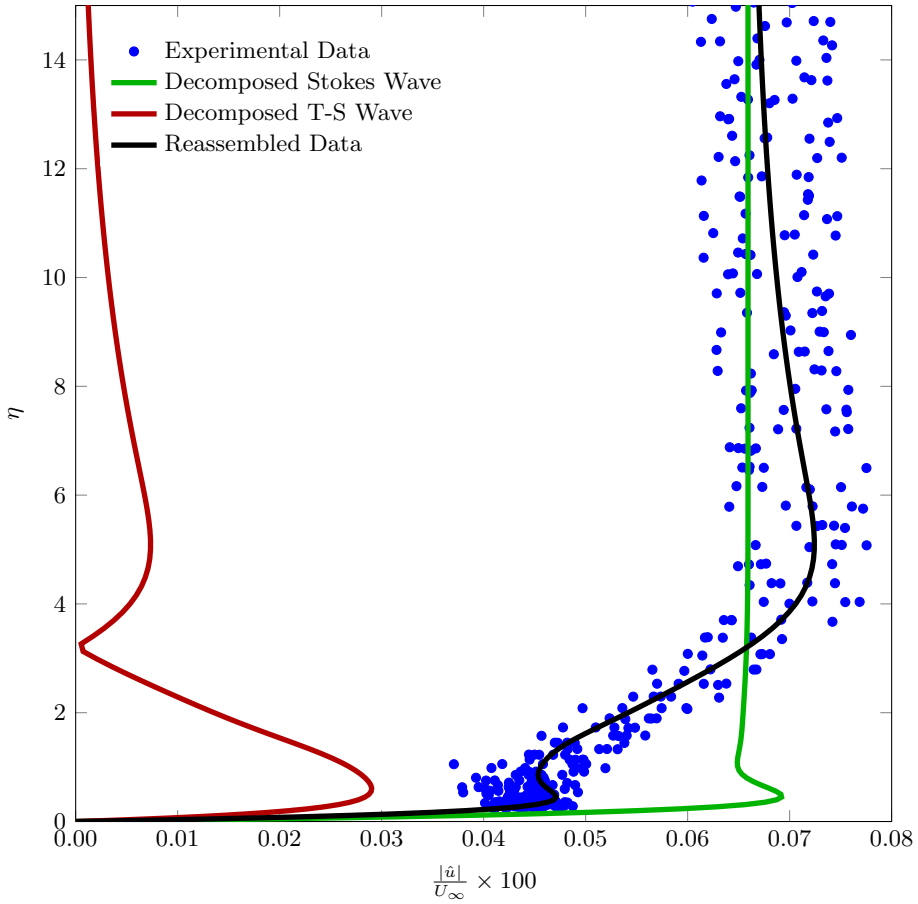

Figure 3. Results from experimental decomposition for $M_\infty = 0.022$, $F = 93.2 \times 10^{-6}$, and $R = 713$. Five experimental boundary-layer scans are shown. The decomposition results presented are the complex average of the individual decompositions.

are very large in comparison to the Stokes waves in this case, a least-squares decomposition method is used to extract the T–S wave amplitude. These experimentally measured T–S wave amplitudes are compared to what linear stability theory predicts in Figure 4.

In Figure 5, the growth of acoustically generated T–S waves, without the tape present, is compared to linear stability theory. In this case, the T–S wave amplitudes are extracted using the biorthogonal decomposition method. There is more spread in the data due to the lower T–S wave amplitudes, and hence, a lower signal-to-noise ratio. Nevertheless, the agreement remains quite good.

Figure 6 displays the experimentally measured acoustic receptivity coefficients for a 20:1 MSE leading edge along with the DNS results of Wanderley & Corke[10] for the same geometry and Reynolds number, $R_b = 2430$. Each point is the result of the experimental decomposition method applied to an individual boundary-layer scan. Unlike the continuous forcing results of Saric et al.,[3] the receptivity curve shows no frequency selection effect. The frequency with maximum acoustic receptivity is equivalent to the results of Wanderley & Corke.[10] However, the maximum experimental acoustic receptivity coefficient is approximately twice the amplitude. There is a small drop in the receptivity curve near $F = 67 \times 10^{-6}$ which is not present in the DNS results. In addition, the experimental receptivity curve may be increasing with frequency around $F = 110 \times 10^{-6}$, though further investigation was not possible due to traverse constraints.

V. Conclusions

Boundary-layer receptivity to freestream acoustic disturbances is fundamental to the origin of T–S waves. Past experiments[3–6] have addressed acoustic receptivity using both continuous forcing and pulsed sound, both of which have problems. In this paper, an experimental biorthogonal decomposition method, coupled

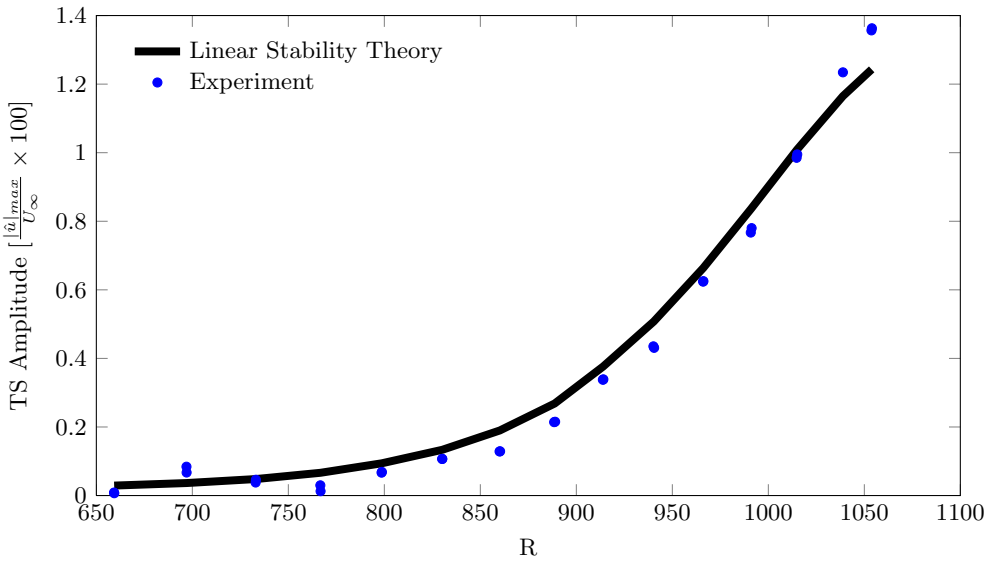

Figure 4. Least-squares decomposition of the growth of T–S waves generated off of Kapton tape placed at the branch I location for $F = (56.8 \pm 0.2) \times 10^{-6}$ compared with linear stability theory.

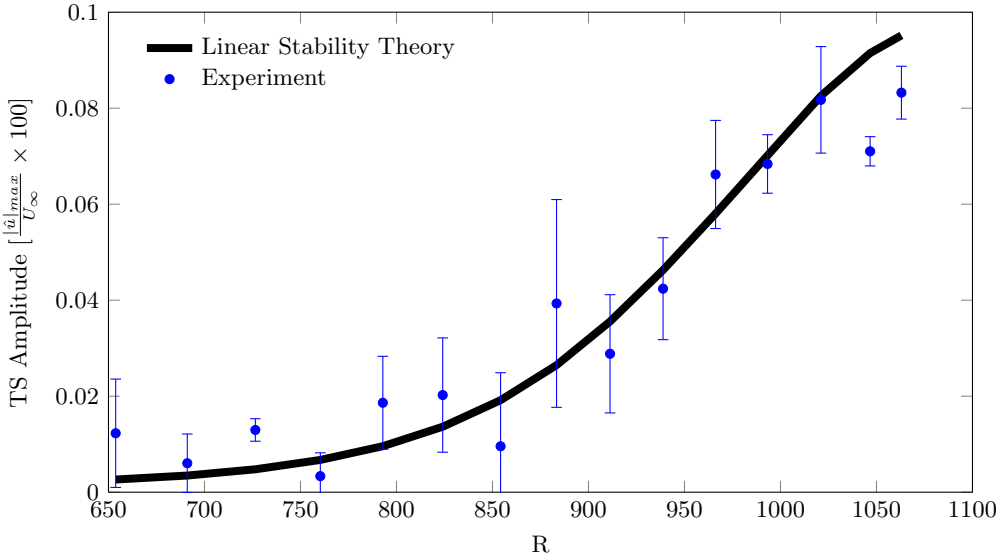

Figure 5. Biorthogonal decomposition of the growth of T–S waves, generated by leading-edge acoustic receptivity, for $F = (60.1 \pm 0.2) \times 10^{-6}$ compared with linear stability theory.

with active noise control, addresses the issues with continuous forcing and enables its use. The experimental decomposition algorithm is able to measure the receptivity coefficient even when only experimental streamwise velocity data is available.

Although the measured receptivity curve differs from the DNS results of Wanderley & Corke[10] in amplitude, the peak occurs at approximately the same nondimensional frequency. Looking at the quality of the individual decompositions, it is clear that the experimental biorthogonal decomposition method is accurately decomposing the experimental fluctuating boundary-layer measurements into T–S and Stokes waves. Even though the active noise control system effectively reduces the amplitude of upstream-traveling sound by 20.4 dB on average, it does not noticeably reduce the global circulation effect. Despite the presence of global circulation, no frequency selection is apparent in the receptivity curve.

Although more work needs to be done to identify and mitigate any additional receptivity sources present

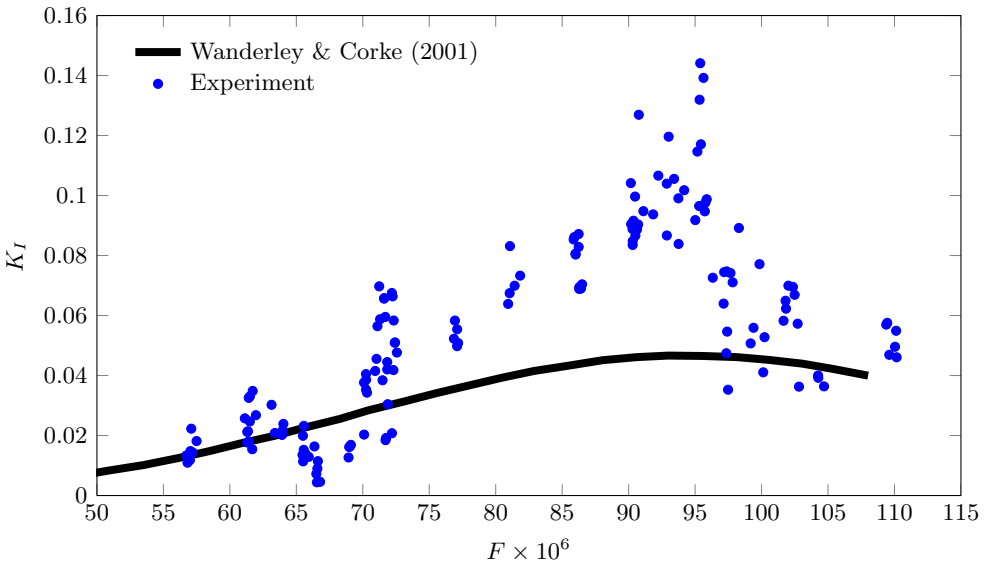

Figure 6. Acoustic receptivity coefficient, experimentally measured and decomposed using biorthogonal decomposition of the modified Orr–Sommerfeld operator. Comparison is made to the acoustic receptivity coefficients obtained through DNS by Wanderley & Corke[10]

in the experiment, the biorthogonal decomposition method has proven to be a powerful method to separate Stokes and T–S waves. The biorthogonality condition is not only applicable in experiments, but could also be utilized in future DNS acoustic receptivity studies to separate the Stokes and T–S waves. Future work will extend the modified O–S equation and the associated biorthogonality condition to flows with non-zero pressure gradients. This will allow the application of the decomposition method to the experimental studies of more complex geometries, such as parabolic leading edges at non-zero angles of attack.

Appendix

The Modified Orr–Sommerfeld (O–S) operators (for a two-dimensional disturbance on a two-dimensional incompressible basic state) are given below. The dilation effect has been added to the continuity equation and can be seen in the fourth row of $\mathcal{A}$ and the third and fourth row of $\mathcal{B}$. The conventional O–S operators are obtained by setting $M_\infty = 0$.

$$\mathcal{A} = diag\left(1, 1, 1, 1 + \frac{iM_\infty^2}{R}\left(\alpha U - RF\right), 0, 0\right)$$

$$\mathcal{B} = \begin{bmatrix} 0 & 1 & 0 & 0 & 0 & 0 \\ iR\left(\alpha U - RF\right) & 0 & R\frac{\partial U}{\partial \eta} & iR\alpha & -i\alpha & 0 \\ -i\alpha & 0 & 0 & -iM_\infty^2\left(\alpha U - RF\right) & 0 & 0 \\ 0 & -\frac{i\alpha}{R} & -i\left(\alpha U - RF\right) & -\frac{i\alpha}{R}M_\infty^2\frac{\partial U}{\partial \eta} & 0 & \frac{i\alpha}{R} \\ i\alpha & 0 & 0 & 0 & -1 & 0 \\ 0 & 0 & i\alpha & 0 & 0 & -1 \end{bmatrix}$$

Biorthogonality Condition

By taking the integral of $\psi_{\alpha'}$ multiplied by Eq. (1), a biorthogonality condition is derived.[20] First, the O–S operators are factored:

$$\mathcal{A} = \mathcal{A}_1 + i\alpha\mathcal{A}_2$$

$$\mathcal{B} = \mathcal{B}_1 + i\alpha\mathcal{B}_2$$

Using this factorization, the integral then becomes: $(D \equiv \partial/\partial\eta)$

$$\int_0^\infty \vec{\psi}_{\alpha'}^T \left(\mathcal{A}_1 + i\alpha\mathcal{A}_2\right) D\vec{\phi}_\alpha d\eta = \int_0^\infty \vec{\psi}_{\alpha'}^T \left(\mathcal{B}_1 + i\alpha\mathcal{B}_2\right) \vec{\phi}_\alpha d\eta$$

After integrating by parts, rearranging terms, and using the definition of the adjoint, Eq. (4), the above equation is simplified and an inner product is defined:

$$\left\langle \vec{\phi}_\alpha, \vec{\psi}_{\alpha'} \right\rangle \Big|_0^\infty = \int_0^\infty \left[D\vec{\psi}_{\alpha'}^T \mathcal{A}_2 + \vec{\psi}_{\alpha'}^T \left(\mathcal{B}_2 + D\mathcal{A}_2\right)\right] \vec{\phi}_\alpha d\eta$$

$$i(\alpha - \alpha') < \vec{\phi}_\alpha, \vec{\psi}_{\alpha'} > \Big|_0^\infty = 0$$

The biorthogonality condition is then given by:

$$< \vec{\phi}_\alpha, \vec{\psi}_{\alpha'} > \Big|_0^\infty = \begin{cases} 0 & \text{for } \alpha \neq \alpha' \\ Q_\alpha & \text{for } \alpha = \alpha' \end{cases}$$

Experimental Decomposition Algorithm

First, the complex Stokes wave amplitude C_{St} is found using a modal assumption and the biorthogonality condition.

$$\vec{\phi}_{exp}^{(0)} = \begin{pmatrix} \hat{u} \\ 0 \\ 0 \\ 0 \\ 0 \\ 0 \end{pmatrix} \qquad \vec{\phi}_{St_{full}} = \begin{pmatrix} \phi_1^{(St)} \\ \phi_2^{(St)} \\ \phi_3^{(St)} \\ \phi_4^{(St)} \\ \phi_5^{(St)} \\ \phi_6^{(St)} \end{pmatrix} \qquad \vec{\phi}_{St_{partial}} = \begin{pmatrix} 0 \\ \phi_2^{(St)} \\ \phi_3^{(St)} \\ \phi_4^{(St)} \\ \phi_5^{(St)} \\ \phi_6^{(St)} \end{pmatrix}$$

$$\vec{\phi}_1 = \begin{cases} C_{St}\vec{\phi}_{St_{full}}, & \text{if } 0 \leq \eta < \eta_b \\ \vec{\phi}_{exp}^{(0)} + C_{St}\vec{\phi}_{St_{partial}}, & \text{if } \eta_b \leq \eta \leq \eta_t \\ C_{St}\vec{\phi}_{St_{full}}, & \text{if } \eta_t < \eta \leq \eta_{max} \end{cases} \tag{6}$$

Plugging Eq. (6) into Eq. (3), the Stokes wave amplitude, C_{St}, is found.

$$C_{St} = \frac{\left\langle \vec{\phi}_{exp}^{(0)}, \vec{\psi}_{St} \right\rangle \Big|_{\eta_b}^{\eta_t}}{Q_{St} - \left\langle \vec{\phi}_{St_{full}}, \vec{\psi}_{St} \right\rangle \Big|_0^{\eta_b} - \left\langle \vec{\phi}_{St_{partial}}, \vec{\psi}_{St} \right\rangle \Big|_{\eta_b}^{\eta_t} - \left\langle \vec{\phi}_{St_{full}}, \vec{\psi}_{St} \right\rangle \Big|_{\eta_t}^{\eta_{max}}} \tag{7}$$

Now that C_{St} has been determined, the Stokes wave is removed from the experimental data:

$$\vec{\phi}_{exp}^{(1)} = \vec{\phi}_{exp}^{(0)} - C_{St} \begin{pmatrix} \phi_1^{(St)} \\ 0 \\ 0 \\ 0 \\ 0 \\ 0 \end{pmatrix}$$

Next, any residual Stokes waves are removed:

$$\vec{\phi}^{(2)}_{exp} = \vec{\phi}^{(1)}_{exp} - mean\left(\phi^{(1)}_{exp_1}\Big|^{\eta=\eta_{max}}_{\eta=33}\right)\begin{pmatrix}\phi^{(St)}_1\\0\\0\\0\\0\\0\end{pmatrix}$$

Now, the T–S wave amplitude, C_{TS}, is found using a T–S wave modal assumption:

$$\vec{\phi}_{TS_{full}} = \begin{pmatrix}\phi^{(TS)}_1\\\phi^{(TS)}_2\\\phi^{(TS)}_3\\\phi^{(TS)}_4\\\phi^{(TS)}_5\\\phi^{(TS)}_6\end{pmatrix} \qquad \vec{\phi}_{TS_{partial}} = \begin{pmatrix}0\\\phi^{(TS)}_2\\\phi^{(TS)}_3\\\phi^{(TS)}_4\\\phi^{(TS)}_5\\\phi^{(TS)}_6\end{pmatrix}$$

$$\vec{\phi}_2 = \begin{cases}C_{TS}\vec{\phi}_{TS_{full}}, & \text{if } 0 \le \eta < \eta_b\\ \vec{\phi}^{(2)}_{exp} + C_{TS}\vec{\phi}_{TS_{partial}}, & \text{if } \eta_b \le \eta \le \eta_t\\ C_{TS}\vec{\phi}_{TS_{full}}, & \text{if } \eta_t < \eta \le \eta_{max}\end{cases}$$

Plugging all of this into Eq. (2), the T–S wave amplitude, C_{TS}, is found.

$$C_{TS} = \frac{\left\langle \vec{\phi}^{(2)}_{exp}, \vec{\psi}_{TS}\right\rangle\Big|^{\eta_t}_{\eta_b}}{Q_{TS} - \left\langle \vec{\phi}_{TS_{full}}, \vec{\psi}_{TS}\right\rangle\Big|^{\eta_b}_{0} - \left\langle \vec{\phi}_{TS_{partial}}, \vec{\psi}_{TS}\right\rangle\Big|^{\eta_t}_{\eta_b} - \left\langle \vec{\phi}_{TS_{full}}, \vec{\psi}_{TS}\right\rangle\Big|^{\eta_{max}}_{\eta_t}} \tag{8}$$

Using Eqs. (7) & (8) outlined above, this new experimental decomposition algorithm is able to accurately decompose an experimental boundary-layer scan into the constituent Stokes and T–S wave amplitudes within a few percent error.

Acknowledgments

This work was sponsored by the National Center for Hypersonic Laminar-Turbulent Transition Research and supported by NASA and AFOSR through AFOSR grant FA9550-09-1-0341.

References

[1]Morkovin, M., Reshotko, E., and Herbert, T., "Transition in open flow systems-a reassessment," *Bull. Am. Phys. Soc*, Vol. 39, No. 9, 1994, pp. 1882.

[2]Goldstein, M. E., "The evolution of Tollmien–Schlichting waves near a leading edge," *Journal of Fluid Mechanics*, Vol. 127, No. 1, 1983, pp. 59–81.

[3]Saric, W. S., Wei, W., Rasmussen, B. K., and Krutckoff, T. K., "Experiments on leading-edge receptivity to sound," 26^{th} *AIAA Fluid Dynamics Conference, San Diego, CA*, 1995.

[4]Saric, W. S. and White, E. B., "Influence of High-Amplitude Noise on Boundary-Layer Transition to Turbulence," 29^{th} *AIAA Fluid Dynamics Conference*, No. 98-2645, 1998.

[5]Saric, W. S., White, E. B., and Reed, H. L., "Boundary-layer receptivity to freestream disturbances and its role in transition," 30^{th} *AIAA Fluid Dynamics Conference, Norfolk, VA*, 1999.

[6]White, E. B., Saric, W. S., and Radeztsky Jr, R. H., "Leading-edge acoustic receptivity measurements using a pulsed-sound technique," *Laminar-Turbulent Transition*, Vol. 5, 2000, pp. 103–08.

[7]Reed, H. L., Lin, N., and Saric, W. S., "Boundary layer receptivity to sound: Navier-Stokes computations," *Applied Mechanics Reviews*, Vol. 43, 1990, pp. 175.

[8]Lin, N., Reed, H. L., and Saric, W. S., "Effect of leading-edge geometry on boundary-layer receptivity to freestream sound, Instability, Transition, and Turbulence,(Hussaini, M. Y., Kumar, A., and Streett, C. L., eds.)," 1992.

[9]Fuciarelli, D., Reed, H. L., and Lyttle, I., "Direct numerical simulation of leading-edge receptivity to sound," *AIAA journal*, Vol. 38, No. 7, 2000, pp. 1159–1165.

[10]Wanderley, J. B. V. and Corke, T. C., "Boundary layer receptivity to free-stream sound on elliptic leading edges of flat plates," *Journal of Fluid Mechanics*, Vol. 429, 2001, pp. 1–21.

[11]Denissen, N. A., *Roughness-induced Transient Growth: Continuous-spectrum Receptivity and Secondary Instability Analysis*, PhD dissertation, Texas A&M University, 2011.

[12]Hammerton, P. W. and Kerschen, E. J., "Boundary-layer receptivity for a parabolic leading edge," *Journal of Fluid Mechanics*, Vol. 310, 1996, pp. 243–268.

[13]Haddad, O. M., Erturk, E., and Corke, T. C., "Acoustic receptivity of the boundary layer over parabolic bodies at angles of attack," *Journal of Fluid Mechanics*, Vol. 536, 2005, pp. 377–400.

[14]Takagi, S. and Konishi, Y., "Frequency Selection Mechanism of Airfoil Trailing-Edge Noise," *Journal of Aircraft*, Vol. 47, No. 4, 2010, pp. 1111–1116.

[15]Denissen, N. A. and White, E. B., "Continuous spectrum analysis of roughness-induced transient growth," *Physics of Fluids*, Vol. 21, No. 11, 2009, pp. 114105.

[16]Tumin, A., Amitay, M., Cohen, J., and Zhou, M. D., "A normal multimode decomposition method for stability experiments," *Physics of Fluids*, Vol. 8, No. 10, 1996, pp. 2777–2779.

[17]Hunt, L. E., Downs III, R. S., Kuester, M. S., White, E. B., and Saric, W. S., "Flow Quality Measurements in the Klebanoff-Saric Wind Tunnel," 27^{th} *AIAA Aerodynamic Measurement Technology and Ground Testing Conference*, No. 2010-4538, 2010.

[18]Klewicki, J., Saric, W., Marusic, I., and Eaton, J., "Wall-Bounded Flows," *Springer Handbook of Experimental Fluid Mechanics*, edited by C. Tropea, A. Yarin, and J. Foss, Springer Berlin Heidelberg, 2007, pp. 871–907.

[19]Kuester, M. S. and White, E. B., "Acoustic Forcing and Control of Reflected Waves in the Klebanoff-Saric Wind Tunnel," 28^{th} *Aerodynamic Measurement Technology, Ground Testing, and Flight Testing Conference*, No. 2012-2862, 2012.

[20]Tumin, A., "Multimode decomposition of spatially growing perturbations in a two-dimensional boundary layer," *Physics of Fluids*, Vol. 15, No. 9, 2003, pp. 2525–2540.